

THE METAGALACTIC IONIZING BACKGROUND: A CRISIS IN UV PHOTON PRODUCTION OR INCORRECT GALAXY ESCAPE FRACTIONS?

J. MICHAEL SHULL, JOSHUA MOLONEY, CHARLES W. DANFORTH, & EVAN M. TILTON
CASA, Department of Astrophysical & Planetary Sciences,
University of Colorado, Boulder, CO 80309

Draft version November 6, 2018

ABSTRACT

Recent suggestions of a “photon underproduction crisis” (Kollmeier et al. 2014) have generated concern over the intensity and spectrum of ionizing photons in the metagalactic ultraviolet background (UVB). The balance of hydrogen photoionization and recombination determines the opacity of the low-redshift intergalactic medium (IGM). We calibrate the hydrogen photoionization rate (Γ_{H}) by comparing *Hubble Space Telescope* spectroscopic surveys of the low-redshift column density distribution of H I absorbers and the observed ($z < 0.4$) mean Ly α flux decrement, $D_A = (0.014)(1+z)^{2.2}$, to new cosmological simulations. The distribution, $f(N_{\text{HI}}, z) \equiv d^2\mathcal{N}/d(\log N_{\text{HI}})dz$, is consistent with an increased UVB that includes contributions from both quasars and galaxies. Our recommended fit, $\Gamma_{\text{H}}(z) = (4.6 \times 10^{-14} \text{ s}^{-1})(1+z)^{4.4}$ for $0 < z < 0.47$, corresponds to unidirectional LyC photon flux $\Phi_0 \approx 5700 \text{ cm}^{-2} \text{ s}^{-1}$ at $z = 0$. This flux agrees with observed IGM metal ionization ratios (C III/C IV and Si III/Si IV) and suggests a 25-30% contribution of Ly α absorbers to the cosmic baryon inventory. The primary uncertainties in the low-redshift UVB are the contribution from massive stars in galaxies and the LyC escape fraction (f_{esc}), a highly directional quantity that is difficult to constrain statistically. We suggest that both quasars and low-mass starburst galaxies are important contributors to the ionizing UVB at $z < 2$. Their additional ionizing flux would resolve any crisis in photon underproduction.

Subject headings: cosmological parameters — ultraviolet: galaxies — observations — intergalactic medium — quasars: absorption lines

1. INTRODUCTION

One of the most important but poorest known parameters in studies of the intergalactic medium (IGM) and circumgalactic medium (CGM) is the intensity of the metagalactic ionizing ultraviolet background (UVB). This uncertainty is not surprising, considering the strong absorption of extreme ultraviolet (EUV) photons at wavelengths $\lambda \leq 911.753 \text{ \AA}$ by the interstellar medium (ISM). Lacking direct measurements of the metagalactic radiation field in the Lyman continuum (LyC), astronomers rely on indirect probes of photoionizing radiation and theoretical estimates¹ based on the presumed ionizing sources and cosmological radiative transfer. An accurate characterization of this UVB is necessary for modeling the thermal and ionization conditions (Bolton et al. 2014; Boera et al. 2014) of the IGM and CGM, for a census of IGM baryon content (Shull et al. 2012b), and for the ionization corrections needed to derive metallicities (Shull et al. 2014; Werk et al. 2014). For photoionization of hydrogen, helium, and many spectroscopically accessible ions of heavy elements (C, N, O, Ne, Mg, Si, S, Fe) the most important spectral range extends from the hy-

drogen Lyman edge (energies $E \geq 13.6 \text{ eV}$) through the He II continuum ($E \geq 54.4 \text{ eV}$) and into the extreme ultraviolet (EUV) and soft X-ray (100-1000 eV).

The claim of a “photon underproduction crisis” (Kollmeier et al. 2014, hereafter denoted K14) generated considerable anxiety in the extragalactic astronomy community and prompted a re-examination of the assumptions in modeling the EUV background at low redshift. These authors compared predictions from smoothed-particle hydrodynamic (SPH) simulations to observed properties of low-redshift H I (Ly α) absorbers. The balance of hydrogen photoionization and radiative recombination rates sets the opacity of the low-redshift IGM, which can be measured from the distribution of Ly α absorbers in redshift (z) and H I column density, N_{HI} (cm^{-2}). This allows one to infer the unidirectional ionizing photon flux Φ_0 ($\text{cm}^{-2} \text{ s}^{-1}$) and specific intensity I_ν ($\text{erg cm}^{-2} \text{ s}^{-1} \text{ Hz}^{-1} \text{ sr}^{-1}$) of LyC radiation. K14 found that the hydrogen photoionization rate (Γ_{H}) required to match their simulated distribution of H I absorbers was *five* times larger than the value predicted in a recent calculation of the UVB by HM12. They found better agreement with previous estimates of a higher UVB (Shull et al. 1999; HM01) that included significant contributions from galaxies. A large part of the UVB discrepancy can be traced to the anomalously low values at $z < 2$ of the LyC escape fraction, $f_{\text{esc}} = (1.8 \times 10^{-4})(1+z)^{3.4}$, adopted by HM12 for galaxies.

In this paper, we undertake a careful examination of this UVB discrepancy, comparing observations of low- z

michael.shull@colorado.edu, joshua.moloney@colorado.edu,
danforth@colorado.edu, evan.tilton@colorado.edu

¹ UVB models include calculations by Haardt & Madau (1996, 2001, 2012), denoted HM96, HM01 and HM12, Shull et al. (1999), and Faucher-Giguère et al. (2009). HM05 refers to the higher-flux spectrum in a 2005 August update to the Haardt & Madau (2001) “Quasars+Galaxies” spectra, provided for inclusion in the photoionization code CLOUDY. The hydrogen photoionization rates, Γ_{H} , in these models vary by up to a factor of six (see Table 1).

TABLE 1
Hydrogen Photoionization Rates^a

Model Reference	$\Gamma_{\text{H}}(z = 0)$	$\Gamma_{\text{H}}(z = 0.25)$
Haardt & Madau (1996)	4.14×10^{-14}	8.63×10^{-14}
Shull et al. (1999)	6.3×10^{-14}	15×10^{-14}
Haardt & Madau (2001)	10.3×10^{-14}	20.6×10^{-14}
Haardt & Madau (2005)	13.5×10^{-14}	29.1×10^{-14}
Haardt & Madau (2012)	2.28×10^{-14}	5.89×10^{-14}
Faucher-Giguère et al. (2009)	3.84×10^{-14}	7.28×10^{-14}
Shull et al. (2015)	4.6×10^{-14}	12×10^{-14}

^a Hydrogen photoionization rates Γ_{H} (s^{-1}) computed at redshifts $z = 0$ and $z = 0.25$ by various theoretical models.

Ly α absorber to new cosmological simulations². Differences among previous theoretical estimates for the UVB may arise from modeling of the evolution of sources of EUV radiation from galaxies and quasars. We use H I data from our recent surveys of low-redshift Ly α absorbers with UV spectrographs on the *Hubble Space Telescope* (*HST*): the STIS (Space Telescope Imaging Spectrograph) survey of 746 Ly α absorbers (Tilton et al. 2012) and the COS (Cosmic Origins Spectrograph) survey of over 2600 Ly α absorbers (Danforth et al. 2015, updated in July 2015). These surveys give consistent results for the bivariate distribution, $f(N_{\text{HI}}, z) \equiv d^2\mathcal{N}/d(\log N_{\text{HI}})dz$, of absorbers in redshift ($z \leq 0.47$) and H I column density ($12.5 \leq \log N_{\text{HI}} \leq 15.5$).

In Section 2, we describe current estimates of the UVB and low-redshift hydrogen photoionization rates and compare our *HST* surveys of intergalactic H I column densities with new grid-code simulations of the IGM. We calibrate the UVB through its influence on the distribution of H I column densities and the flux decrement (D_A) from Ly α line blanketing. In Section 3, we justify boosting Γ_{H} by a factor of 2–3 above HM12 values, together with other parameters that characterize the UVB: the specific intensity I_0 ($\text{erg cm}^{-2} \text{s}^{-1} \text{Hz}^{-1} \text{sr}^{-1}$) at the Lyman limit and the integrated LyC photon flux Φ_0 ($\text{cm}^{-2} \text{s}^{-1}$). For $0 \leq z \leq 0.47$, our revised ionization rate is $\Gamma_{\text{H}} \approx (4.6 \times 10^{-14} \text{s}^{-1})(1+z)^{4.4}$. At $z = 0$, this corresponds to $\Phi_0 \approx 5700 \text{cm}^{-2} \text{s}^{-1}$ and $I_0 = 1.7 \times 10^{-23} \text{erg cm}^{-2} \text{s}^{-1} \text{Hz}^{-1} \text{sr}^{-1}$. These parameters are in agreement with photoionization modeling in our recent IGM survey (Shull et al. 2014) of metal-ion ratios (C III/C IV and Si III/Si IV). This increase in the UVB is comparable to previous calculations (Shull et al. 1999; HM01, HM05) and likely arises from imprecise modeling of sources of EUV radiation (galaxies and quasars). The larger UVB would be consistent with an increased contribution of galaxies with LyC escape fractions, $f_{\text{esc}} \approx 0.05$ at $z < 2$, in contrast to the very low values $f_{\text{esc}} < 10^{-3}$ adopted by HM12. A recent analysis (Khaire & Srianand 2015) of the effects of a revised QSO luminosity function (Croom et al. 2009; Palanque-DeLabrouille et al. 2013) increased the low-redshift UVB by a factor of two. Both of these results suggest that the

² Our simulations are made with the N-body hydrodynamic grid code *Enzo* (<http://enzo-project.org>). For an overview of the code see Bryan et al. (2014). Our previous applications of *Enzo* to IGM astrophysics appear in Smith et al. (2011), Shull et al. (2012a), and Shull et al. (2012b).

UVB extrapolated to low redshift was under-estimated by HM12 by a factor of approximately 2–3.

2. CONSTRAINING THE UV BACKGROUND

2.1. Definitions and Measurements of the Ionizing Radiation Field

For an isotropic radiation field of specific intensity I_ν , the normally incident *photon flux* per frequency is $(\pi I_\nu/h\nu)$ into an angle-averaged, forward-directed effective solid angle of π steradians. The isotropic photon flux striking an atom or ion is $4\pi(I_\nu/h\nu)$, and the hydrogen photoionization rate follows by integrating this photon flux times the photoionization cross section over frequency from threshold (ν_0) to ∞ .

$$\Gamma_{\text{H}} = \int_{\nu_0}^{\infty} \frac{4\pi I_\nu}{h\nu} \sigma_\nu d\nu \approx \frac{4\pi I_0 \sigma_0}{h(\alpha + 3)}. \quad (1)$$

Here, we approximate the frequency dependence of specific intensity and photoionization cross section by power laws, $I_\nu = I_0(\nu/\nu_0)^{-\alpha}$ and $\sigma_\nu = \sigma_0(\nu/\nu_0)^{-3}$, where $\sigma_0 = 6.30 \times 10^{-18} \text{cm}^2$ and $\alpha \approx 1.4$ for AGN (Shull et al. 2012c; Stevans et al. 2014). The integrated unidirectional flux of ionizing photons is then

$$\Phi_0 = \int_{\nu_0}^{\infty} \frac{\pi I_\nu}{h\nu} d\nu = \frac{\pi I_0}{h\alpha}, \quad (2)$$

which is related to the density of hydrogen-ionizing photons by $\Phi_0 = n_\gamma(c/4)$ for an isotropic radiation field. We then have the relations among parameters:

$$\Gamma_{\text{H}} = 4\sigma_0\Phi_0 \left(\frac{\alpha}{\alpha + 3} \right) = (8.06 \times 10^{-14} \text{s}^{-1})\Phi_4 \quad (3)$$

$$\Gamma_{\text{H}} = \frac{4\pi I_0 \sigma_0}{h(\alpha + 3)} = (2.71 \times 10^{-14} \text{s}^{-1})I_{-23}, \quad (4)$$

where we normalize the incident flux of ionizing photons and specific intensity to characteristic values, $\Phi_0 = (10^4 \text{cm}^{-2} \text{s}^{-1})\Phi_4$ and $I_0 = (10^{-23} \text{erg cm}^{-2} \text{s}^{-1} \text{Hz}^{-1} \text{sr}^{-1})I_{-23}$ at the hydrogen Lyman limit ($h\nu_0 = 13.60 \text{eV}$). In an *HST*/COS survey of IGM metallicity at $z \leq 0.4$, Shull et al. (2014) found that $\Phi_4 \approx 1$ and $I_{-23} \approx 3$ gave reasonable fits to the observed ratios of adjacent ionization states of carbon and silicon, $(\text{Si III}/\text{Si IV}) = 0.67_{-0.19}^{+0.35}$, $(\text{C III}/\text{C IV}) = 0.70_{-0.20}^{+0.43}$, and their sum, $(\Omega_{\text{CIII}} + \Omega_{\text{CIV}})/(\Omega_{\text{SiIII}} + \Omega_{\text{SiIV}}) = 4.9_{-1.1}^{+2.2}$.

Over the past 20 years, numerous papers have estimated the ionizing background and photoionization rate. Table 1 lists Γ_{H} for several models, with values at $z = 0$ ranging from $(2.28 - 13.5) \times 10^{-14} \text{s}^{-1}$. The HM12 rate, $\Gamma_{\text{H}} = 2.28 \times 10^{-14} \text{s}^{-1}$, corresponds to a one-sided ionizing flux $\Phi_0 = [\Gamma_{\text{H}}(\alpha + 3)/4\sigma_0\alpha] \approx 2630 \text{cm}^{-2} \text{s}^{-1}$ and specific intensity $I_{-23} \approx 0.823$ for the radio-quiet AGN spectral index ($\alpha = 1.57$) assumed by HM12. These fluxes are lower by a factor of three compared to the $z = 0$ metagalactic radiation fields from AGN and galaxies calculated by Shull et al. (1999), $I_{\text{AGN}} = 1.3_{-0.5}^{+0.8} \times 10^{-23}$ and $I_{\text{Gal}} = 1.1_{-0.7}^{+1.5} \times 10^{-23}$, respectively. Adding these two values with propagated errors gives a total intensity and hydrogen ionization rate of $I_{\text{tot}} = 2.4_{-0.9}^{+1.7} \times 10^{-23} \text{erg cm}^{-2} \text{s}^{-1} \text{Hz}^{-1} \text{sr}^{-1}$ and $\Gamma_{\text{H}} = 6.0_{-2.1}^{+4.2} \times 10^{-14} \text{s}^{-1}$. The difference between

TABLE 2
Column Density Distribution^a (STIS Survey)

$\langle \log N_{\text{HI}} \rangle$	Range in $\log N_{\text{HI}}$	\mathcal{N}_{abs}	Δz_{eff}	$f(N_{\text{HI}}, z)$
13.0	(12.9–13.1)	115	4.637	124_{-13}^{+13}
13.2	(13.1–13.3)	115	5.003	115_{-11}^{+11}
13.4	(13.3–13.5)	106	5.216	102_{-10}^{+10}
13.6	(13.5–13.7)	75	5.327	70_{-8}^{+9}
13.8	(13.7–13.9)	73	5.341	68_{-8}^{+9}
14.0	(13.9–14.1)	50	5.360	47_{-7}^{+7}
14.2	(14.1–14.3)	35	5.379	33_{-5}^{+6}
14.4	(14.3–14.5)	26	5.382	24_{-5}^{+6}
14.6	(14.5–14.7)	18	5.382	17_{-4}^{+5}

^a For 613 low-redshift Ly α absorbers taken from *HST*/STIS survey (Tilton et al. 2012), the columns show: (1) mean column density (N_{HI} in cm^{-2}) with bin width $\Delta \log N_{\text{HI}} = 0.2$; (2) bin range in $\log N_{\text{HI}}$; (3) number of Ly α absorbers (\mathcal{N}_{abs}) in bin; (4) total redshift pathlength Δz_{eff} at each N_{HI} ; (5) bivariate distribution of absorbers in column density and redshift, $f(N_{\text{HI}}, z) \equiv d^2\mathcal{N}/d(\log N_{\text{HI}})dz$, computed as $(\mathcal{N}_{\text{abs}}/0.2\Delta z_{\text{eff}})$ and plotted in Figures 2–7.

these radiation fields appears to be the contribution from galaxies. The HM12 background adopts a negligible UVB from galaxies, whereas the background models of Shull et al. (1999), HM01, and HM05 have comparable intensities from galaxies, owing to higher assumed LyC escape fractions.

2.2. *HST* Observations of the H I Column Density Distribution

Previous ultraviolet spectroscopic surveys of low-redshift Ly α absorbers estimated their contribution to the baryon census through the distribution of H I column densities in the diffuse Ly α forest (e.g., Penton et al. 2000, 2004; Lehner et al. 2007; Danforth & Shull 2008). Our recent *HST* surveys of the low-redshift IGM were more extensive, obtaining 746 Ly α absorbers with STIS (Tilton et al. 2012) and 2577 Ly α absorbers with COS (Danforth et al. 2015). The COS survey used the medium-resolution far-UV gratings (Green et al. 2012) with coverage between 1135–1460 Å (G130M) and 1390–1795 Å (G160M); a few spectra extended slightly outside these boundaries. Our COS survey probed 82 AGN sight lines with cumulative pathlength $\Delta z = 21.7$ with H I column densities N_{HI} (in cm^{-2}) between $12.5 < \log N_{\text{HI}} < 17$. For this paper, we analyze a “uniform redshift-limited sample” of Ly α absorbers at $z \leq 0.47$. As discussed in these survey papers, the Ly α statistics are consistent with 24–30% of the baryons residing in the Ly α forest and partial Lyman-limit systems.

Table 2 summarizes the data selected from the STIS survey, with 613 Ly α absorbers at $z \leq 0.4$ over the range $12.9 \leq \log N_{\text{HI}} \leq 14.7$, reprocessed as described in Danforth et al. (2015). Table 3 gives similar results from the COS survey at $z \leq 0.47$, with 2074 absorbers between $12.6 \leq \log N_{\text{HI}} \leq 15.2$. For each bin in $\log N_{\text{HI}}$, we list the number of absorbers (\mathcal{N}_{abs}) and effective redshift pathlength (Δz_{eff}) over which our Ly α survey is sensitive. From these data, we derive the bivariate distribution, $d^2\mathcal{N}/d(\log N_{\text{HI}})dz$, of absorbers in H I column density and redshift by dividing \mathcal{N}_{abs} by Δz_{eff} and

TABLE 3
Column Density Distribution^a (COS Survey)

$\langle \log N_{\text{HI}} \rangle$	Range in $\log N_{\text{HI}}$	\mathcal{N}_{abs}	Δz_{eff}	$f(N_{\text{HI}}, z)$
12.7	(12.6–12.8)	194	3.67	260_{-120}^{+1000}
12.9	(12.8–13.0)	292	9.79	150_{-40}^{+80}
13.1	(13.0–13.2)	383	16.46	120 ± 10
13.3	(13.2–13.4)	368	18.78	98 ± 5
13.5	(13.4–13.6)	267	19.23	69_{-12}^{+17}
13.7	(13.6–13.8)	146	12.03	61 ± 5
13.9	(13.8–14.0)	123	12.25	50 ± 5
14.1	(14.0–14.2)	96	12.96	37 ± 4
14.3	(14.2–14.4)	75	13.75	27_{-3}^{+4}
14.5	(14.4–14.6)	47	14.17	17_{-2}^{+3}
14.7	(14.6–14.8)	45	14.24	16_{-2}^{+3}
14.9	(14.8–15.0)	19	14.25	$6.7_{-1.5}^{+1.9}$
15.1	(15.0–15.2)	19	14.25	$6.7_{-1.5}^{+1.9}$

^a Statistics of low-redshift Ly α absorbers ($12.6 \leq \log N_{\text{HI}} < 15.2$) taken from the *HST*/COS survey (Danforth et al. 2015, updated July 2015) using the “uniform sub-sample” of 2074 H I absorbers. The columns show: (1) mean column density (N_{HI} in cm^{-2}) with bin width $\Delta \log N_{\text{HI}} = 0.2$; (2) bin range in $\log N_{\text{HI}}$; (3) number of Ly α absorbers (\mathcal{N}_{abs}) in bin; (4) total redshift pathlength Δz_{eff} at each N_{HI} ; (5) bivariate distribution of absorbers in column density and redshift, $f(N_{\text{HI}}, z) \equiv d^2\mathcal{N}/d(\log N_{\text{HI}})dz$, computed as $(\mathcal{N}_{\text{abs}}/0.2\Delta z_{\text{eff}})$ and plotted in Figures 2–7.

$\Delta \log N_{\text{HI}} = 0.2$. An accurate calculation of this distribution function requires both good absorber counting statistics and knowledge of the pathlength Δz_{eff} covered in the survey for a given column density. As in Danforth & Shull (2008), we compute Δz_{eff} corresponding to the 4σ minimum Ly α equivalent width as a function of wavelength in each spectrum. Asymmetric error bars arise from statistical uncertainties in \mathcal{N}_{abs} and Δz_{eff} , computed for each bin using the formalism of Gehrels (1986). At low column densities, the errors are dominated by Δz_{eff} , while at high column densities the errors are dominated by the small values of \mathcal{N}_{abs} in bins at $\log N_{\text{HI}} \geq 14.6$.

An important effect of the IGM is the flux decrement, D_A , produced by Ly α forest line blanketing of the continuum flux. Previous measurements of D_A were reported by Kirkman et al. (2007) using low-resolution UV observations with the *HST* Faint Object Spectrograph (FOS) toward 74 AGN. Their measured decrements were fitted to a power law, $D_A(z) = (0.016)(1+z)^{1.01}$, over the range $0 < z < 1.6$ with considerable scatter. Based on our moderate-resolution *HST*/COS survey, Figure 1 shows the fraction of light removed by Ly α absorption from the continuum for $0 < z < 0.47$. These statistics were found by summing the *observed-frame* equivalent widths of all identified ($> 4\sigma$) Ly α absorbers in the Danforth et al. (2015) catalog within a given redshift range, normalized by the effective redshift pathlength probed by the survey for absorbers of that strength. The uncertainty, σ_{D_A} , is the quadratic sum of measured equivalent-width uncertainties normalized in the same manner. The errors are small at lower redshifts ($z \lesssim 0.35$) where most of the surveyed Ly α absorbers are found. However, they remain small compared to D_A even at higher redshifts where Δz_{eff} is smaller. Figure 1 shows our results for bins of width $\Delta z = 0.01$ and $\Delta z = 0.05$ to illustrate the vari-

ance on small scales. The scatter in D_A is significantly larger than σ_{D_A} , and cosmic variance is significant, particularly at $z > 0.35$. These fluctuations are large in the $\Delta z = 0.01$ bins, which are comparable to the mean absorber separations for the observed Ly α absorption-line frequencies $dN/dz \approx 100 - 200$ for $\log N_{\text{HI}} = 12.7 - 13.3$.

Figure 1 shows a small dip in D_A between $0.2 < z < 0.3$. This redshift band corresponds to Ly α absorbers at 1459 Å to 1580 Å, observed primarily by the COS/G160M grating (1390–1795 Å) since G130M ends at 1460 Å. The dip appears in several ranges of column density, $13 < \log N_{\text{HI}} < 14$ and $14 < \log N_{\text{HI}} < 15$. The first range is expected to dominate line blanketing in the Ly α forest for line profiles with Doppler velocity parameters $b \approx 25 - 30 \text{ km s}^{-1}$. The dip also remains when we offset the redshift bins. Thus, we believe the dip to be real, although we do not have a plausible physical explanation for its presence.

We fitted the mean values of the *HST* observations with $\Delta z = 0.05$ bins to the power-law form $D_A(z) = (0.014 \pm 0.001)(1+z)^{2.2 \pm 0.2}$. For $z \leq 0.2$, these observations are in reasonable agreement with the lower-resolution *HST*/FOS results of Kirkman et al. (2007), although we find steeper redshift evolution. By post-processing the H I absorption-line profiles in our simulations (Sections 2.3 and 2.4) over the range $0 < z < 0.2$, we find mean decrements at $\langle z \rangle = 0.1$ of $D_A = 0.0116$, 0.0097, and 0.0332 for the HM01, HM05, and HM12 radiation fields, respectively. At $\langle z \rangle = 0.1$, these UVBs correspond to hydrogen photoionization rates $\Gamma_{\text{H}} = 3.54 \times 10^{-14} \text{ s}^{-1}$ (HM12), $1.38 \times 10^{-13} \text{ s}^{-1}$ (HM01), and $1.86 \times 10^{-13} \text{ s}^{-1}$ (HM05). Our simulations find that $D_A \propto \Gamma_{\text{H}}^{-0.7}$. In their SPH simulations, K14 found decrements at $z \approx 0.1$ of $D_A = 0.024$ (HM01) and $D_A = 0.050$ (HM12), higher than our simulations by factors of 1.9 and 2.9, respectively. Similar offsets are seen in the distribution of H I column densities.

Our observations at $z \leq 0.47$ with STIS (Tilton et al. 2012) and COS (Danforth et al. 2015) yield consistent values for $f(N_{\text{HI}}, z)$, the bivariate distribution of Ly α absorbers in column density and redshift. A least-squares fit of the COS data over the range $12.7 \leq \log N_{\text{HI}} \leq 15.2$ had the form, $f(N_{\text{HI}}, z) \equiv d^2N/d(\log N_{\text{HI}})dz \approx (167)N_{13}^{-0.65 \pm 0.02}$, where we define the dimensionless column density $N_{13} = [N_{\text{HI}}/10^{13} \text{ cm}^{-2}]$. We can use this line frequency to make an analytic estimate of the Ly α line blanketing and flux decrement,

$$D_A = \int_{N_1}^{N_2} \left(\frac{W_\lambda}{\lambda} \right) f(N, z) d(\log N) \\ = \left(\frac{\pi e^2 f \lambda}{m_e c^2} \right) \left(\frac{167 \times 10^{13} \text{ cm}^{-2}}{2.303} \right) \int_{N_1}^{N_2} N_{13}^{-0.65} dN_{13} \quad (5)$$

In the last expression of Equation (5), we assume unsaturated Ly α lines, with equivalent widths $W_\lambda/\lambda = (\pi e^2/m_e c)(N f \lambda/c)$, where W_λ and $\lambda = 1215.67 \text{ \AA}$ are defined in the rest-frame and $f = 0.4164$ is the Ly α oscillator strength. We adopt limits $\log N_1 = 12.5$ and $\log N_2 = 14.0$ for the integral, which we denote $I(N_1, N_2) \approx 4.49$. The estimated decrement $D_A = (0.00323)I(N_1, N_2) \approx 0.0145$, close to our observations at $z \approx 0$. Because line frequency $f(N_{\text{HI}}, z) \propto (1+z)^{2.2}$

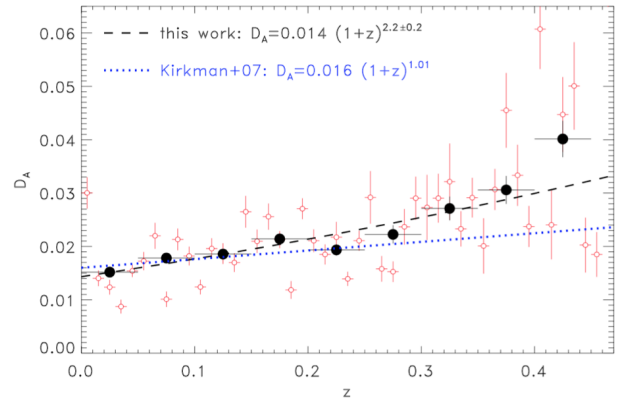


FIG. 1.— Flux decrement from the Danforth et al. (2015) low- z IGM survey with COS (updated in July 2015) showing the fraction of flux removed from the continuum by Ly α absorbers for redshifts $0 < z < 0.47$. The decrement $D_A(z)$ is calculated from the normalized, summed, observed-frame equivalent widths of Ly α absorbers in a given redshift bin, divided by the effective pathlength (Δz_{eff}) probed by the survey at each redshift. Red open circles show D_A in bins of width $\Delta z = 0.01$. Filled black circles show D_A in bins of $\Delta z = 0.05$ and fitted to $D_A(z) = (0.014)(1+z)^{2.2 \pm 0.2}$ (dashed line). Blue dotted line shows the fit, $D_A(z) \approx (0.016)(1+z)^{1.01}$, found by Kirkman et al. (2007) in lower-resolution *HST*/FOS measurements. The small drop in D_A at $z \approx 0.2 - 0.3$ appears over several column-density ranges and remains when we shift redshift bins.

out to $z \approx 0.5$ (Danforth et al. 2015), we expect D_A to have the same dependence, as seen in Figure 1. This calculation shows that for the observed steep distribution of H I column densities, most of the line blanketing occurs from moderate-strength Ly α absorbers at $N_{\text{HI}} \approx N_2$, beginning to saturate and appear on the flat portion of the curve of growth. Owing to line saturation, the stronger but rarer Ly α absorbers add a small amount to this estimate.

2.3. Cosmological Simulations of H I in the low- z IGM

Our simulations of the H I absorber distributions were run using the Eulerian N-body + hydrodynamics code *Enzo* (Bryan et al. 2014). The N-body dynamics of the dark matter particles in our simulations were calculated using a particle-mesh solver (Hockney & Eastwood 1988), and the hydrodynamic equations were solved using a direct-Eulerian piecewise parabolic method (Colella & Woodward 1984; Bryan et al. 1995) with a Harten-Lax-van Leer-Contact Riemann solver (Toro et al. 1994). Our modifications of this code and its applications to the IGM are discussed in Smith et al. (2011), where we conducted tests of convergence, examined various feedback schemes, and compared the results to IGM thermal phases, O VI absorbers, and star-formation histories using box sizes of $25h^{-1} \text{ Mpc}$ and $50h^{-1} \text{ Mpc}$ and grids of 256^3 , 384^3 , 512^3 , 768^3 , and 1024^3 cells. We note that the Smith et al. (2011) simulations used the HM96 background, rather than HM01 as stated in that paper³. This code has a

³ Because the HM96 background is 2.5 times lower than HM01, the Ly α forest was stronger in the Smith et al. (2011) simulations. However, as we discuss in Section 2.4, the HM96 background is

substantial IGM heritage, with applications to O VI absorbers (Smith et al. 2011), the baryon census at $z < 0.4$ (Shull et al. 2012b), clumping factors and critical star-formation rates during reionization (Shull et al. 2012a), and synthetic absorption-line spectra for comparison of simulations with *HST* observations (Egan et al. 2014).

Our current simulations were initialized at a redshift $z = 99$ and run to $z = 0$, using the WMAP-9 maximum likelihood concordance values (Hinshaw et al. 2013) with $\Omega_m = 0.282$, $\Omega_\Lambda = 0.718$, $\Omega_b = 0.046$, $H_0 = 69.7 \text{ km s}^{-1} \text{ Mpc}^{-1}$, $\sigma_8 = 0.817$, and $n_s = 0.965$ to create the initial conditions. The dark matter density power spectrum used the Eisenstein & Hu (1999) transfer function. Three independent realizations of the initial conditions were created in order to constrain the effects of cosmic variance due to the finite box size. Two of the realizations were created using MUSIC (Hahn & Abel 2011) with second-order Lagrangian perturbation theory. The third realization was created using the initial condition generator packaged with *Enzo*. The basic simulations discussed in this paper were run on static, uniform grids with a box size of $50h^{-1}$ comoving Mpc and 512^3 and 768^3 cells. We also analyzed a previous simulation with 1536^3 cells, produced by Britton Smith on the XSEDE supercomputer and discussed in our study of IGM clumping factors (Shull et al. 2012a), as well the ($1024^3, 50h^{-1}$ Mpc) simulations of Smith et al. (2011). Because those 1024^3 models were run with an older UVB from Haardt & Madau (1996), we chose not to compare them to our 512^3 and 768^3 runs, which used more recent backgrounds (HM01, HM05, HM12).

In view of the different predictions of our code for the distribution of low-redshift Ly α absorbers, it is appropriate to compare the resolution⁴ of our grid-code simulations to the SPH simulations run by K14. With a co-moving box size of $50h^{-1}$ Mpc, our models have spatial resolutions (cell sizes) of $97.6h^{-1}$, $65.1h^{-1}$, and $32.6h^{-1}$ kpc for grids of 512^3 , 768^3 , and 1536^3 , respectively. The corresponding dark-matter mass resolutions are $m_{\text{dm}} = 6.1 \times 10^7 h^{-1} M_\odot$ (512^3), $1.8 \times 10^7 h^{-1} M_\odot$ (768^3), and $2.2 \times 10^6 h^{-1} M_\odot$ (1536^3). For comparison, the simulations analyzed by K14 used the SPH code of Davé et al. (2010), also in a $50h^{-1}$ Mpc box with 576^3 dark-matter (and baryon) particles. The characteristic spatial resolution in their SPH method is the interparticle distance, $50h^{-1} \text{ Mpc}/576 \approx 86.8h^{-1}$ kpc. Under gravitational evolution, the SPH particles are concentrated in regions with baryon overdensity $\Delta_b = \rho_b/\bar{\rho}_b > 1$, and the interparticle distance is reduced by a factor of $\Delta_b^{1/3}$. Although K14 do not quote a mass resolution, their simulation ($50h^{-1}$ Mpc, 576^3) would have $m_{\text{dm}} \approx 5 \times 10^7 h^{-1} M_\odot$, scaling from values quoted in the ($512^3, 100h^{-1}$ Mpc) SPH calculation of Tepper-Garcia et al. (2012).

close to the value we recommend in our current study. Consequently, our 2011 simulations are in reasonable agreement with the *HST* observations of the low-redshift Ly α forest.

⁴ The original study by Davé et al. (2010) used simulations in a $48h^{-1}$ Mpc box, and most of their studies were run with 384^3 particles. To investigate effects of numerical resolution and box size, they also employed a simulation with 512^3 particles in a $96h^{-1}$ Mpc box. Contemporaneous SPH studies (Tepper-Garcia et al. 2012) of the IGM were conducted by the ‘‘Overwhelmingly Large Simulations’’ (OWLS) project (Schaye et al. 2010) in a $100h^{-1}$ Mpc box with 512^3 dark-matter (and baryon) particles.

Therefore, the mass resolution in our 512^3 runs is comparable to that of K14, and our 768^3 and 1536^3 resolutions are superior. Resolution can be important when applied to the large (100-200 kpc) Ly α absorption systems observed in the low-redshift IGM.

Star particles were formed in the simulations using the subgrid physics prescription of Cen & Ostriker (1992). Star formation occurs in cells where the baryon density is greater than 100 times the critical density, the divergence of the velocity is negative, and the cooling time is less than the dynamical time. As described by Smith et al. (2011), we adopted a star formation efficiency of 10% in these cells. Feedback from star formation returns gas, matter, and energy from star particles to the ISM and IGM. Although star particles are formed instantaneously, feedback occurs gradually with an exponential decay over time. Star particles produce 90% of their feedback within four dynamical times of their creation. Of the star particles’ total mass, 25% is returned as gas, with 10% of that taking the form of metals and 10^{-5} of the rest-mass energy returned as thermal feedback. The feedback is distributed evenly over 27 grid cells centered on the star particle. This scheme avoids the overcooling and subsequent runaway star formation that occurs when feedback is returned to a single cell. We analyzed this ‘‘distributed feedback’’ method in our previous study (Smith et al. 2011) and found that it produces better convergence and removes the over-cooling. These simulations were able to reproduce both the observed star-formation history and the number density of O VI absorbers per unit redshift over the range $0 < z < 0.4$. Many SPH studies of the IGM (Davé et al. 2010; Tepper-Garcia et al. 2012) suppress the over-cooling by suspending the cooling or turning off the hydrodynamics for a period of time, allowing the injected energy and metals to diffuse into the surrounding gas.

The ionization states of H and He in the IGM were calculated with the non-equilibrium chemistry module in *Enzo* (Abel et al. 1997; Anninos et al. 1997). Metal cooling of the gas was computed using precompiled CLOUDY⁵ (Ferland 2013) tables that assume ionization equilibrium for the metals and are coupled to the chemistry solver (Smith et al. 2008). Photoionization and radiative heating of the gas come from a spatially uniform metagalactic UVB. For each realization of the initial conditions, we ran three simulations that were identical except for the form of the UVB. Two simulations used analytic fits to the HM01 and HM05 backgrounds, initialized at $z = 8.9$ and reaching full strength by $z = 8$. A third background used the HM12 table implemented in the *Grackle*⁶ chemistry and cooling library (Bryan et al. 2014; Kim et al. 2014) that begins at $z = 15.13$.

In order to analyze the distribution of Ly α absorbers in the simulations, we created synthetic quasar sight lines using the YT⁷ analysis package (Turk et al. 2011). For each simulation box, we created 200 synthetic sight lines, each constructed from simulation outputs spanning the redshift range $0.0 \leq z \leq 0.4$. A randomly oriented ray was chosen through each output, representing the portion of the sight line beginning at the output redshift

⁵ <http://nublado.org>

⁶ <https://grackle.readthedocs.org/>

⁷ <http://yt-project.org>

and with sufficient pathlength to cover the Δz to the next output file. These rays were then combined to create a sight line spanning the entire redshift range. We used identical random seeds for simulations sharing the same initial conditions; differences in the absorber distributions therefore directly reflect effects of different ultraviolet backgrounds. Each sight line is composed of many line elements, from the portions of the sight line passing through a single grid cell. We identified Ly α absorbers as sets of contiguous line elements with neutral hydrogen density $n_{\text{HI}} \geq 10^{-12.5} \text{ cm}^{-3}$. Egan et al. (2014) compared this method of identifying absorbers to a more sophisticated method involving synthetic spectra. In their Figure 11, they showed that the resulting absorber column density distributions are in good agreement. We also analyzed a large ($1536^3, 50h^{-1}$ Mpc) simulation run by Britton Smith and discussed in Shull et al. (2012a). The light rays from this simulation were generated by Devin Silvia, and we analyzed them in the same manner.

2.4. Comparison of Simulations with Observations

The flux decrement D_A is an imperfect metric for estimating the UVB, since measurements of the observed flux decrement depend on spectral resolution. In addition, both measurements and simulations exhibit significant variance in D_A . A more robust IGM diagnostic comes from the distribution of H I column densities. Figure 2 illustrates the observed STIS and COS distributions, $f(N_{\text{HI}}, z)$, over the range $12.5 \leq \log N_{\text{HI}} \leq 14.5$. The STIS and COS bins are offset by $\Delta \log N_{\text{HI}} = 0.1$, using data from Tables 2 and 3. The COS survey is more extensive in both absorber numbers and column density, and its statistical accuracy is superior to that of the STIS survey. Over the overlapping range in $\log N_{\text{HI}}$, the agreement is good. We over-plot values of $f(N_{\text{HI}}, z)$ from our new IGM simulations ($50h^{-1}$ Mpc box and 768^3 grid cells) using three different ionizing backgrounds (HM01, HM05, HM12). As analyzed further in Section 2.5, the inferred baryon density requires ionization corrections for the neutral fraction, $n_{\text{HI}}/n_{\text{H}}$. Appendix A suggests that the amplitude of the Ly α absorber distribution, $f(N_{\text{HI}}, z)$, is proportional to $\Gamma_{\text{H}}^{-1/2} T_4^{-0.363}$ for fixed baryon content (Ω_b) and temperature $T = (10^4 \text{ K}) T_4$, and it therefore provides a constraint on the UVB. In our simulations, we find that $f(N_{\text{HI}}, z) \propto \Gamma_{\text{H}}^{-0.773}$ for absorbers in the range $13 < \log N_{\text{HI}} < 14$.

Figures 2–7 illustrate the differential absorber distribution, $d^2 N/d(\log N_{\text{HI}}) dz$, with tests of convergence, cosmic variance, box size, feedback, and redshift evolution. The simulated distributions are compared to observed distributions from *HST* surveys of Tilton et al. (2012) and Danforth et al. (2015). Figure 2 presents the primary results of this paper: the H I column-density distributions for three radiation fields (HM01, HM05, HM12) computed with 768^3 grids and a $50h^{-1}$ Mpc box. The lower HM12 background produces significantly more absorbers than earlier UVBs, ranging from a factor of two for absorbers between $12.5 \leq \log N_{\text{HI}} \leq 12.7$ to a factor of seven for $14.3 \leq \log N_{\text{HI}} \leq 14.5$. The observed distributions fall between the results for the HM01 and HM12 backgrounds, approaching the HM12 simulations for $\log N_{\text{HI}} > 14.0$. This suggests that there may be less tension between the HM12 background and observations

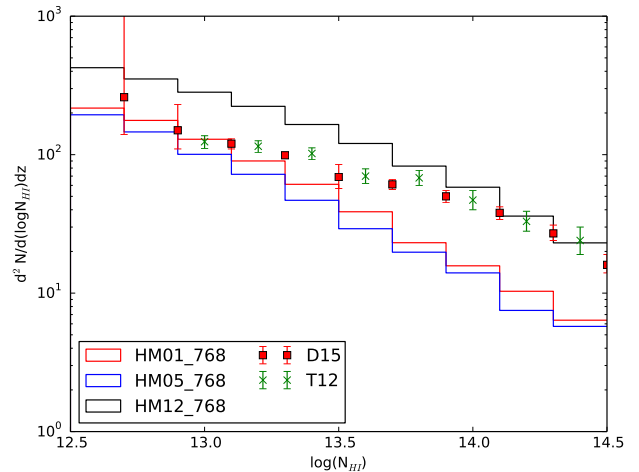


FIG. 2.— *HST* surveys of the column-density distribution of low-redshift IGM absorbers are compared to new cosmological simulations with the *Enzo* grid code (768^3 cells, $50h^{-1}$ Mpc box) with three ionizing UV backgrounds (HM01, HM05, HM12). We plot the bivariate distribution of absorbers, $f(N_{\text{HI}}, z) = d^2 N/d(\log N_{\text{HI}}) dz$, in redshift and column density (N_{HI} in cm^{-2}) with $\Delta \log N_{\text{HI}} = 0.2$ bins. Data from *HST*/COS survey (D15: Danforth et al. 2015) are shown as red squares, and data from *HST*/STIS survey (T12: Tilton et al. 2012) as green crosses. Analytic theory (Appendix A) shows that, for fixed baryon content, Ly α line frequency scales with photoionization rate and gas temperature as $\Gamma_{\text{H}}^{-1/2} T_4^{-0.363}$. The HM12 simulations use a lower ionizing flux and produce a higher absorption-line density. For data with the best statistics ($13 \leq \log N_{\text{HI}} \leq 14$), the observed distribution, $f(N_{\text{HI}}, z) \approx (167)[N_{\text{HI}}/10^{13} \text{ cm}^{-2}]^{-0.65}$, lies between simulations run with higher UVB (HM01 and HM05) and the lower HM12 background, except at the highest column densities. The best-fit distribution requires an ionizing background approximately 2-3 times higher than HM12, but with sufficient uncertainty that a crisis in photon production is unlikely.

than implied by the K14 results. Figure 3 explores effects of cosmic variance, comparing three models with $50h^{-1}$ Mpc boxes and 512^3 grids. For each radiation field (HM01, HM05, HM12) the simulations labeled with subscripts 1 and 2 are those with the MUSIC initial conditions, and those labeled 3 use the *Enzo*-packaged initial conditions. For a fixed UVB the scatter among simulations is at the 15% level or less, indicating that variance is unlikely to play an important role. Figure 4 explores convergence of our simulations, comparing models with $50h^{-1}$ Mpc boxes on grids of 512^3 , 768^3 , and 1536^3 . The differences between these models are relatively small, at the 10% level and within the expected differences arising from sample variance. Figure 5 investigates the potential effects of box size, which could suppress structure formation down to low redshift if the box was too small. We ran two simulations ($100h^{-1}$ Mpc, 512^3 and $50h^{-1}$ Mpc, 256^3), both using the same HM01 ionizing background. The grid cell sizes are identical ($195h^{-1}$ kpc), and the results are essentially the same for $\log N_{\text{HI}} < 14$.

Figure 6 explores the potential influence of our feedback methods. In our 512^3 simulations, feedback has

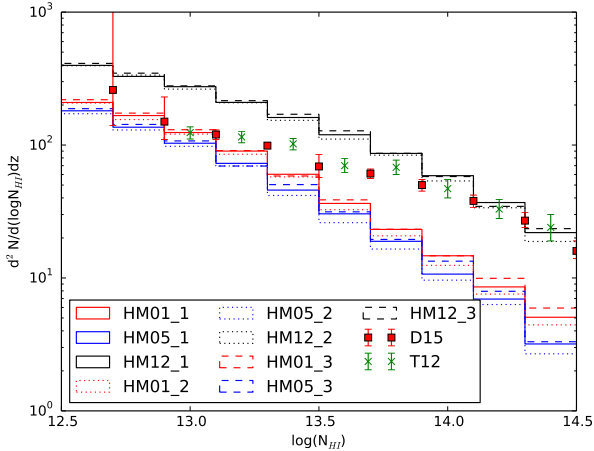


FIG. 3.— Same format as Figure 2. To test cosmic variance, we show three ($50h^{-1}$ Mpc, 512^3) simulations for each UVB, labeled HM01- i , HM05- i , and HM12- i (subscripts $i = 1, 2, 3$ correspond to runs with different initial conditions) and compared to *HST* survey data (D15 and T12).

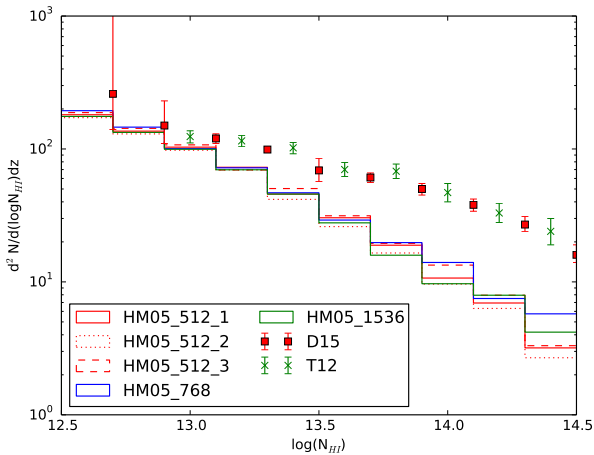


FIG. 4.— Same format as Figure 2. To test convergence, we compared three ($50h^{-1}$ Mpc, 512^3) simulations, labeled as HM05- i (subscripts $i = 1, 2, 3$) with two larger simulations: a new 768^3 simulation (HM05_768) and the 1536^3 simulation (HM05_1536) provided by Britton Smith and first presented in Shull et al. (2012). All used the same (HM05) ionizing radiation field and are compared to *HST* spectroscopic survey data from STIS (T12) and from COS (D15).

little effect on the distribution of H I column densities. We find little difference if we inject mass, metals, and energy within a single cell, in adjacent cells, or eliminating feedback entirely. Clumpiness of the IGM on small scales can be affected by the feedback method, even though the large-scale structural parameters, (T , ρ_b) and (Δ_b , N_{HI}), remain nearly the same. Figure 7 investigates the possible effects of redshift evolution of the Ly α forest. We split the simulated results into two redshift intervals ($0 < z < 0.2$ and $0.2 < z < 0.4$) in our 768^3 simulations, all run with the HM01 radiation field. Differences between the simulated distributions are quite small and

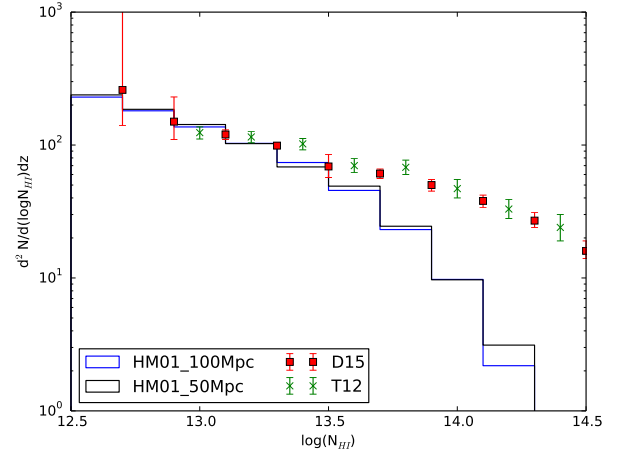


FIG. 5.— Same format as Figure 2. To test effects of box size, we show two simulations, one at ($100h^{-1}$ Mpc, 512^3) and another at ($50h^{-1}$ Mpc, 256^3), both using the HM01 ionizing background. Results are compared to our *HST* survey data (D15 and T12). The grid cell sizes are identical ($195h^{-1}$ kpc), and the results are essentially the same for $\log N_{\text{HI}} < 14$. The roll-off in simulated absorbers at $\log N_{\text{HI}} > 13.7$ is an artifact of the poor resolution in these runs.

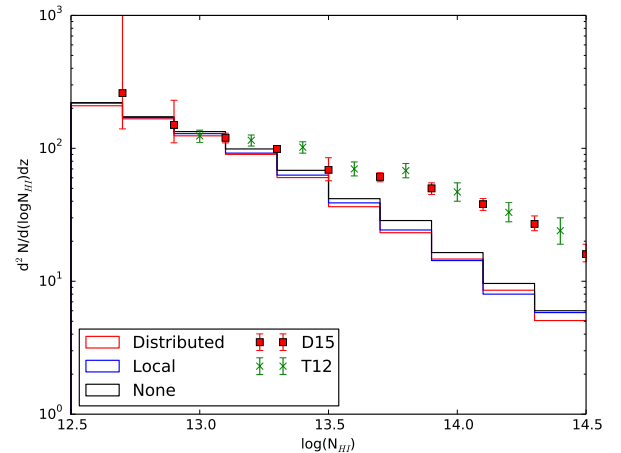


FIG. 6.— Same format as Figure 2. To test effects of feedback injection methods, we show three ($50h^{-1}$ Mpc, 512^3) simulations following the feedback prescriptions of Smith et al. (2011). We explored distributed feedback (into the adjoining 27 cells), local feedback (into a single cell), and no feedback from star formation. All simulations are run with the same HM01 radiation field and compared to *HST* survey data (D15 and T12).

consistent with COS observations (Danforth et al. 2015), in which the weak Ly α absorbers ($\log N_{\text{HI}} < 14$) exhibit little redshift evolution between $z = 0$ and $z = 0.4$.

2.5. Comparisons to Previous Simulations

To compare our grid-code simulations with previous SPH models, we examined two structural measures of the IGM. The first measure is the thermal-phase diagram of (T , ρ_b), the temperature vs. baryon density in the low-

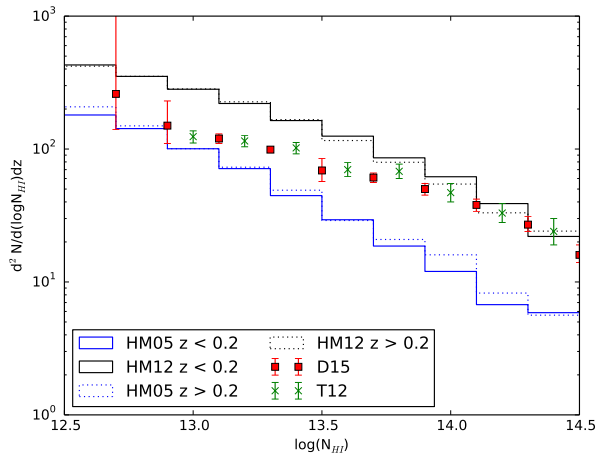


FIG. 7.— Same format as Figure 2. To test for redshift evolution of the low-redshift Ly α forest, we split the results into two redshift intervals ($0 < z < 0.2$ and $0.2 < z < 0.4$) for 768³ simulations, run with both HM05 and HM12 radiation fields. Evolution in the distribution of weak Ly α absorbers in the *HST* survey (D15 and T12) are small, differing by less than 5% between $0 < z < 0.4$.

redshift Ly α forest. For our grid models, these diagrams were shown as Figure 19 in Smith et al. (2011) and as Figure 1 in Shull et al. (2012b). For the SPH models, we examined Figure 8 of Davé et al. (2010) and Figure 7 of Tepper-Garcia et al. (2012). All of these diagrams are consistent with a relation $T = (5000 \text{ K}) \Delta_b^{0.6}$ where Δ_b is the baryon overdensity. A second measure is the correlation of baryon overdensity and column density (Δ_b, N_{HI}), typically expressed as a power-law, $\Delta_b = \Delta_0 N_{14}^\alpha$, where Δ_0 is the normalization at a fiducial H I column density $N_{\text{HI}} = (10^{14} \text{ cm}^{-2}) N_{14}$. These correlations vary with redshift, but typically are evaluated at $z = 0.25$. Davé et al. (2010) used (384³, 48 h^{-1} Mpc) simulations with the HM01 background to derive a fit for absorbers with $T < 10^{4.5}$ K,

$$\Delta_b = (35.5 \pm 0.03) N_{14}^{0.741 \pm 0.003} f_\tau^{-0.741} 10^{-0.365z}. \quad (6)$$

Here, $f_\tau \approx 2/3$ is a renormalization factor of optical depths introduced to multiply the simulated optical depths to match the mean flux decrement D_A . Thus, at $z = 0.25$ and with $f_\tau \approx 2/3$, they found $\Delta_b = (38.9) N_{14}^{0.741}$. From (512³, 100 h^{-1} Mpc) simulations with the HM01 background, Tepper-Garcia et al. (2012) found $\Delta_b = (48.3) N_{14}^{0.786 \pm 0.010}$, with no renormalization factor f_τ . They noted a theoretical expectation that $\Delta_b \propto N_{\text{HI}}^{0.738}$ for absorbing gas in hydrostatic and photoionization equilibrium (Schaye 2001). In our (768³, 50 h^{-1} Mpc) simulations, also using the HM01 radiation field, we find $\Delta_b = (36.9) N_{14}^{0.65}$ over the range $0.2 < z < 0.3$ for column densities $12.5 < \log N_{\text{HI}} < 14.5$. The overdensity is calculated as a weighted average over the line elements that make up the absorber, using the column density as the weight field. We find similar normalizations, $\Delta_0 = (36.9, 38.9, 48.3)$ for the three simulations (Shull et al. 2015, Davé et al. 2010, Tepper-Garcia et al. 2012) evaluated at $z = 0.25$ with the HM01 background.

Evidently, the structural measures of the low- z Ly α forest give similar results. The thermal-phase diagrams are essentially identical, while the differences in the (Δ_b, N_{HI}) correlation likely arise from different methods of identifying and characterizing H I absorbers in column density and over-density. These comparisons are complicated by the fact that Davé et al. (2010) corrected their simulated optical depths by a factor (f_τ), and Tepper-Garcia et al. (2012) corrected for the temperature-density correlation of gas in hydrodynamic and photoionization equilibrium. The simulations also used different cosmological parameters. Tepper-Garcia et al. (2012) adopted density fractions ($\Omega_m = 0.238$ and $\Omega_b = 0.0418$) from WMAP-3, which are lower by 15.6% and 9.1% than our WMAP-9 values ($\Omega_m = 0.282$ and $\Omega_b = 0.046$). Davé et al. (2010) adopted WMAP-7 parameters ($\Omega_m = 0.28$ and $\Omega_b = 0.046$) similar to our values. Kollmeier et al. (2014) used $\Omega_m = 0.25$ (10% lower than our value) and $\Omega_b = 0.044$ (4.3% lower). The simulations also have different resolutions: our standard simulations use (768³, 50 h^{-1} Mpc) while Tepper-Garcia use (512³, 100 h^{-1} Mpc). Given the scatter in these correlations, their redshift dependence, and the correction factors, the modest differences do not warrant concern.

3. SUMMARY: A HIGHER UV BACKGROUND?

Using our recent *HST* spectroscopic surveys of intergalactic Ly α absorbers, we have characterized their distribution in H I column density and redshift. By comparing the observed distribution to new *Enzo* simulations of the low-redshift IGM, we find an ionizing background *intermediate* between the HM01 and HM12 values. As shown in Appendix A, the inferred baryon density and absorption-line frequency depend inversely on the UVB and temperature, scaling as $\Gamma_{\text{H}}^{-1/2} T^{-0.363}$. To fit the the *HST* data, we require approximately a factor of 2–3 increase in the photoionization rate above HM12, somewhat less than the factor of five suggested by K14. However, no single UVB agrees with the full distribution. Figure 2 suggests that a higher UVB is needed to explain the line frequency of weak absorbers ($12.7 < \log N < 13.9$), while the lower HM12 background is consistent with the distribution of stronger absorbers ($\log N_{\text{HI}} > 14$). Given the uncertainties in source emissivities, cosmological radiative transfer, and galaxy LyC escape fractions, our H I results do not constitute a crisis in our understanding of the sources of the UVB.

We have explored a number of potential explanations for the differences between the H I distributions produced by various simulations and their sub-grid feedback schemes, gaseous sub-structure, and injection of mass and metals. In photoionized Ly α absorbers, the neutral hydrogen density depends on n_{H}^2 . Consequently, the UVB and photoionization rate needed to explain the amplitude of $f(N_{\text{HI}}, z)$ may be sensitive to the clumping factor, $C_{\text{H}} \equiv \langle n_{\text{H}}^2 \rangle / \langle n_{\text{H}} \rangle^2$. However, a detailed code comparison is beyond the scope of what we can do at this time. In the comparisons discussed earlier, we demonstrated that the integrated column densities, N_{HI} , are less sensitive to the procedures for identifying absorbers or the feedback schemes. After investigating convergence, cosmic variance, and feedback, we conclude that the differences must arise elsewhere.

The primary influence on the distribution of H I absorbers in the Ly α forest is the ionizing radiation field. A larger UVB was also found in calculations that included contributions from both quasars and galaxies (Shull et al. 1999; Faucher-Giguère et al. 2009). The primary uncertainties in the UVB are the contribution from massive stars in galaxies (Topping & Shull 2015) and the LyC escape fraction (HM12; Benson et al. 2013), a highly directional quantity that is difficult to constrain statistically from direct observations. The parameterization adopted by HM12, $f_{\text{esc}} = (1.8 \times 10^{-4})(1+z)^{3.4}$, was tuned to match observations at $z > 2.5$, but it is likely much too low at $z < 2$ where observational constraints are rare. Reliable values require direct measurements of LyC fluxes from a statistically significant sample ($N_{\text{gal}} \gg 20$) of starburst galaxies to constrain the low escape fractions expected from a highly directional LyC escape geometry. For example, if theoretical models predict $\langle f_{\text{esc}} \rangle \approx 0.05$, with 5% of the LyC escaping from each side of a gaseous disk through perpendicular conical chimneys (Dove & Shull 1994), direct detections would be possible, on average, in only 5% of the observations. Constraints on f_{esc} will require large samples to deal with inclination bias. Such a situation is seen in direct-detection observations at $z \approx 3$ (Shapley et al. 2006; Nestor et al. 2013; Mostardi et al. 2013) and at $z \approx 0.2$ (Heckman et al. 2011) which find either large (10-40%) fractions of transmitted LyC flux or none at all. The difficulties with low- z constraints on f_{esc} were discussed by Shull et al. (2014) in their low- z census of IGM metal abundances and ionization ratios ($\text{C}^{+3}/\text{C}^{+2}$ and $\text{Si}^{+3}/\text{Si}^{+2}$).

We therefore suggest that starburst galaxies are important contributors to the ionizing UVB at $z < 2$. Their contribution to the ionizing background would explain the observed distribution of Ly α absorbers and could resolve the discrepancy in IGM photoheating inferred from the opacity of the Ly α forest at $z < 2$ (Puchwein et al. 2015). It has also been suggested that TeV emission from blazars could add significant heat to the IGM through pair-production of high-energy electrons and positrons (Puchwein et al. 2012). We have not investigated their effects on our data, either on $D_A(z)$ or the distribution in H I column density. We summarize the main results of our study as follows:

1. Compared to **Enzo** N-body hydrodynamical simulations of the low- z IGM with different values of the ionizing UV background, the observed distribution of Ly α forest absorbers ($z < 0.5$) lies intermediate between the HM01 and HM12 background calculations. A fit to the observations requires a factor-of-two increase in the UVB above HM12 with a recommended hydrogen ionization rate $\Gamma_{\text{H}}(z) = (4.6 \times 10^{-14} \text{ s}^{-1})(1+z)^{4.4}$.
2. The one-sided ionizing photon flux $\Phi_0 \approx 5700 \text{ cm}^{-2} \text{ s}^{-1}$ at $z = 0$ agrees with the observed IGM metal ionization ratios, C III/C IV and Si III/Si IV (Shull et al. 2014), and suggests a 25–30% contribution of Ly α absorbers to the cosmic baryon inventory.

3. The increased ionizing background probably requires an increase in the escape fraction of ionizing (LyC) radiation from starburst galaxies above the low values ($f_{\text{esc}} < 10^{-3}$) adopted by HM12. Ionizing photons from galaxies with $\langle f_{\text{esc}} \rangle \approx 0.05$ gives results consistent with previous UVB modeling (Shull et al. 1999) that found similar contributions from AGN and starburst galaxies, with specific intensities ($\text{erg cm}^{-2} \text{ s}^{-1} \text{ Hz}^{-1} \text{ sr}^{-1}$) at 13.6 eV of $I_{\text{AGN}} = 1.3_{-0.5}^{+0.8} \times 10^{-23}$ and $I_{\text{Gal}} = 1.1_{-0.7}^{+1.5} \times 10^{-23}$.
4. Because LyC propagation through the ISM is expected to be highly directional, detections of escaping photons depend on galaxy orientation and will require large surveys to obtain valid statistical inferences.

Future observational and theoretical work could significantly improve our characterization of the ionizing UVB at $z < 1$. We need better accuracy of the column-density distribution of Ly α absorbers at $\log N_{\text{HI}} \leq 13.0$ and $\log N_{\text{HI}} \geq 14.5$. Larger surveys of IGM absorbers will allow us to measure the redshift evolution of the distribution, $d^2N/d(\log N_{\text{HI}})dz$, to test the expected increase in photoionization rate, $\Gamma_{\text{H}}(z) \propto (1+z)^{4.4}$. The most critical future experiment will be direct measurements of LyC escape fractions from a large sample of starburst galaxies at $z < 0.4$.

This work was supported by NASA grant NNX08AC14G for COS data analysis and STScI archival grant AR-11773.01-A. We appreciate the efforts of Britton Smith and Devin Silvia in providing the light rays from unpublished **Enzo** 1536³ models computed on the XSEDE supercomputer and used to construct column density distributions. We thank Ben Oppenheimer, Ewald Puchwein, Martin Haehnelt, Mark Giroux, and John Stocke for helpful discussions. This work utilized the *Janus* supercomputer, operated by the University of Colorado and supported by the National Science Foundation (award number CNS-0821794), the University of Colorado Boulder, the University of Colorado Denver, and the National Center for Atmospheric Research. Computations described in this work were performed using the publicly-available **Enzo** code (<http://enzo-project.org>), which is the product of a collaborative effort of many independent scientists from numerous institutions around the world.

REFERENCES

- Abel, T., Anninos, P., Zhang, Y., & Norman, M. L. 1997, *New Astr.*, 2, 181
- Ade, P. A. R., (Planck Collaboration), et al. 2014, *A&A*, 571, A16
- Anninos, P., Zhang, Y., Abel, T., & Norman, M. L. 1997, *New Astr.*, 2, 209
- Benson, A., Venkatesan, A., & Shull, J. M. 2013, *ApJ*, 770, 76
- Boera, E., Murphy, M. T., Becker, G. D., & Bolton, J. S. 2014, *MNRAS*, 441, 1916
- Bolton, J. S., Becker, G. D., Haehnelt, M. G., & Viel, M. 2014, *MNRAS*, 438, 2499
- Bryan, G. L., Norman, M. L., Stone, J. M., et al. 1995, *Comp. Phys. Comm.*, 89, 149
- Bryan, G. L., Norman, M. L., O’Shea, B. W., et al. 2014, *ApJS*, 211, 19
- Cen, R., & Ostriker, J. P. 1992, *ApJ*, 399, L113
- Colella, P., & Woodward, P. R. 1984, *J. Comp. Phys.* 54, 174
- Croom, S. M., Richards, G. T., Shanks, T., et al. 2009, *MNRAS*, 399, 1755
- Danforth, C. W., & Shull, J. M. 2008, *ApJ*, 679, 194
- Danforth, C. W., Tilton, E. M., Shull, J. M., et al. 2015, *ApJ*, submitted (arXiv:1402.2655) (D15)
- Davé, R., Oppenheimer, B. D., Katz, N., et al. 2010, *MNRAS*, 408, 2051
- Dove, J. B., & Shull, J. M. 1994, *ApJ*, 430, 222
- Egan, H., Smith, B. D., O’Shea, B. W., & Shull, J. M. 2014, *ApJ*, 791, 64
- Eisenstein, D. J., & Hu, W. 1999, *ApJ*, 511, 5
- Faucher-Giguère, C.-A., Lidz, A., Zaldarriaga, M., & Hernquist, L. 2009, *ApJ*, 703, 1416
- Ferland, G., Porter, R., van Hoof, P. A. M., et al. 2013, *Rev Mex A&A*, 49, 137
- Gehrels, N. 1986, *ApJ*, 303, 336
- Green, J. C., Froning, C. S., Osterman, S., et al. 2012, *ApJ*, 744, 60
- Haardt, F., & Madau, P. 1996, *ApJ*, 461, 20
- Haardt, F., & Madau, P. 2001, in *Clusters of Galaxies and the High Redshift Universe Observed in X-rays*, ed. D. M. Neumann & J. T. V. Tran, (Saclay: CEA), 64 (arXiv:astro-ph/0106018)
- Haardt, F., & Madau, P. 2012, *ApJ*, 746, 125
- Hahn, O., & Abel, T. 2011, *MNRAS*, 415, 2101
- Heckman, T. M., Borthakur, S., Overzier, R., et al. 2011, *ApJ*, 730, 5
- Hinshaw, G., Larson, D., Komatsu, E., et al. 2013, *ApJS*, 208, 19
- Hockney, R. W., & Eastwood, J. W. 1988, *Computer Simulation Using Particles*, (Bristol: Taylor & Francis, Ltd)
- Khairé, V., & Srikanand, R. 2015, *MNRAS*, 451, L30
- Kim, J.-H., Abel, T., Agertz, O., et al. 2014, *ApJS*, 210, 14
- Kirkman, D., Tytler, D., Lubin, D., & Charlton, J. 2007, *MNRAS*, 376, 1227
- Kollmeier, J. A., Weinberg, D. H., Oppenheimer, B. D., et al. 2014, *ApJ*, 789, L32 (K14)
- Lehner, N., Savage, B. D., Richter, P., et al. 2007, *ApJ*, 658, 680
- Mostardi, R. E., Shapley, A. E., Nestor, D. B., et al. 2013, *ApJ*, 779, 65
- Nestor, D. B., Shapley, A. E., Kornei, K. A., Steidel, C. C., & Siana, B. 2013, *ApJ*, 765, 47
- Palanque-Delabrouille, N., Magnaville, Ch., Yèche, Ch., et al. 2013, *A&A*, 551, 29
- Penton, S. V., Shull, J. M., & Stocke, J. T. 2000, *ApJ*, 544, 150
- Penton, S. V., Stocke, J. T., & Shull, J. M. 2004, *ApJS*, 152, 29
- Puchwein, E., Bolton, J. S., Haehnelt, M. G., et al. 2015, *MNRAS*, 450, 4081
- Puchwein, E., Pfrommer, C., Springel, V., Broderick, A. E., & Chang, P. 2012, *MNRAS*, 423, 149
- Schaye, J. 2001, *ApJ*, 559, 507
- Schaye, J., Dalla Vecchia, C., Booth, C. M., et al. 2010, *MNRAS*, 402, 1536
- Shapley, A. E., Steidel, C. C., Pettini, M., Adelberger, K. L., & Erb, D. K. 2006, *ApJ*, 651, 688
- Shull, J. M., Danforth, C. W., & Tilton, E. M. 2014, *ApJ*, 796, 49
- Shull, J. M., Harness, A., Trenti, M., & Smith, B. D. 2012a, *ApJ*, 747, 100
- Shull, J. M., Roberts, D., Giroux, M. L., Penton, S. V., & Fardal, M. A. 1999, *AJ*, 118, 1450
- Shull, J. M., Smith, B. D., & Danforth, C. W. 2012b, *ApJ*, 759, 23
- Shull, J. M., Stevans, M. L., & Danforth, C. W. 2012c, *ApJ*, 752, 162
- Smith, B. D., Hallman, E., Shull, J. M., & O’Shea, B. 2011, *ApJ*, 731, 6
- Smith, B. D., Sigurdsson, S., & Abel, T. 2008, *MNRAS*, 385, 1443
- Stevans, M. L., Shull, J. M., Danforth, C. W., & Tilton, E. M. 2014, *ApJ*, 794, 75
- Tepper-Garcia, T., Richter, P., Schaye, J., et al. 2012, *MNRAS*, 425, 1640
- Tilton, E. M., Danforth, C. W., Shull, J. M., & Ross, T. L. 2012, *ApJ*, 759, 112 (T12)
- Topping, M. W., & Shull, J. M. 2015, *ApJ*, 800, 97
- Toro, E. F., Spruce, M., & Speares, W. 1994, *Comp. Phys. Comm.*, 4, 25
- Turk, M. J., Smith, B. D., Oishi, J. S., et al. 2011, *ApJS*, 192, 9
- Werk, J. K., Prochaska, J. X., Tumlinson, J., et al. 2014, *ApJ*, 792, 8

4. APPENDIX A: DEPENDENCE OF Ly α ABSORBERS ON IONIZATION RATE

The intergalactic Ly α absorbers are thought to arise as fluctuations in dark-matter confined clumps or filaments. Modeling their distribution and frequency throughout intergalactic space depends on the cosmological evolution of this gas, coupled to calculations of the “neutral fraction”, $f_{\text{HI}} \equiv n_{\text{HI}}/n_{\text{H}}$, produced by the balance of photoionization and radiative recombination. These physical processes can be modeled by N-body hydrodynamic simulations, but one can also derive their general behavior through simple analytic arguments (Shull et al. 2012b). Here, we describe the key assumptions and parameters to illustrate how the baryon density and hydrogen ionization rate Γ_{H} can be inferred from observations of the H I column density distribution and the frequency, dN/dz , of absorbers per unit redshift.

We assume a distribution of IGM absorbers with constant co-moving space density, $\phi(z) = \phi_0(1+z)^3$, and constant cross section πp^2 . We adopt a cosmological relation between proper distance and redshift, $dl/dz = c(dt/dz) = [c/(1+z)H(z)]$, where the Hubble parameter at redshift z in a flat Λ CDM cosmology is $H(z) = H_0[\Omega_m(1+z)^3 + \Omega_\Lambda]^{1/2}$. In this model, the frequency of absorbers is $dN/dz = [c/(1+z)H(z)]\pi p^2\phi(z)$. The internal density distributions of the absorbers are approximated as singular isothermal spheres, and the IGM baryon density and H I fractions follow from photoionization models that translate the observed H I to total hydrogen. To compare with observations, we integrate through the cloud along a chord at impact parameter $p = (100 \text{ kpc})p_{100}$ of the AGN sight line through the absorber. We adopt a 100-kpc characteristic scale length of Ly α absorbers, normalized at fiducial H I column density $N_{\text{HI}} = (10^{14} \text{ cm}^{-2})N_{14}$. Because most Ly α -forest absorbers are low density and optically thin in their Lyman lines, we use a case-A hydrogen recombination rate coefficient, $\alpha_{\text{H}}^{(A)} = (4.09 \times 10^{-13} \text{ cm}^3 \text{ s}^{-1})T_4^{-0.726}$, scaled to temperature $T = (10^4 \text{ K})T_4$. For nearly fully ionized H and He, with helium abundance $y = n_{\text{He}}/n_{\text{H}} \approx 1/12$ by number, we adopt electron density $n_e = (1 + 2y)n_{\text{H}}$ and mean baryon mass per hydrogen $\mu_b = (1 + 4y)m_{\text{H}}$.

The co-moving baryon mass density of Ly α absorbers of column density N_{HI} , probed at impact parameter p , is the product of absorber space density,

$$\phi(z) = \frac{(dN/dz)H(z)(1+z)}{(\pi p^2)c}, \quad (7)$$

and absorber mass

$$M_b(p) = 4\pi\mu_b p^{5/2} \left[\frac{2\Gamma_{\text{H}}(z) N_{\text{HI}}(p)}{\pi(1+2y)\alpha_{\text{H}}^{(A)}} \right]^{1/2}. \quad (8)$$

The co-moving mass density, $\rho_b = \phi_0 M_b \propto [p N_{\text{HI}} \Gamma_{\text{H}}]^{1/2} (dN/dz)$, is then integrated over the distribution in H I column density. We normalize ρ_b to the closure parameter, $\Omega_b^{(\text{HI})} = \rho_b/\rho_{\text{cr}}$ at redshift $z = 0$, relative to critical density $\rho_{\text{cr}} = (3H_0^2/8\pi G)$. Because our *HST* surveys extend to $z \approx 0.5$, we must include the cosmological evolution in $H(z)$, $\phi(z)$, and $\Gamma_{\text{H}}(z)$. Before introducing these corrections, we outline the method at low redshift, for which the Euclidean calculation gives

$$\Omega_b^{(\text{HI})} = \left[\frac{32(2\pi)^{1/2}}{3} \right] \left(\frac{dN}{dz} \right) \left(\frac{G\mu_b}{cH_0} \right) \left[\frac{p N_{\text{HI}} \Gamma_{\text{H}}}{\alpha_{\text{H}}^{(A)}(1+2y)} \right]^{1/2} = (7.1 \times 10^{-3}) \left[\frac{dN/dz}{100} \right] \left[p_{100} N_{14} \left(\frac{\Gamma_{\text{H}}}{\Gamma_{\text{HM12}}} \right) \right]^{1/2} h_{70}^{-1} T_4^{0.363}. \quad (9)$$

Here, we normalize the Ly α frequency to a characteristic value $dN/dz = 100$ and scale Γ_{H} to the HM12 ionization rate, $\Gamma_{\text{HM12}} = (2.28 \times 10^{-14} \text{ s}^{-1})(1+z)^{4.4}$, which we fitted over the range $0 < z < 0.7$. The weak temperature dependence comes from the recombination rate coefficient. The coefficient (7.1×10^{-3}) corresponds to $\sim 15\%$ of the cosmological baryon fraction, $\Omega_b = 0.0463 \pm 0.00093$ (Hinshaw et al. 2013; Ade et al. 2014). For fixed baryon density $\Omega_b^{(\text{HI})}$ in the Ly α forest, the *observed* frequency of Ly α absorbers, $dN/dz \propto \Gamma_{\text{H}}^{-1/2}$, scaling as the inverse square root of the ionizing background.

Our *HST* surveys of Ly α absorbers provide accurate values of $\Omega_b^{(\text{HI})}$, based on an integration over the column-density distribution. After inserting the redshift corrections to $\phi(z)$, $H(z)$, and $\Gamma_{\text{H}}(z)$, we derive a general expression for $\Omega_b^{(\text{HI})}$,

$$\Omega_b^{(\text{HI})} = (7.1 \times 10^{-5}) \left[\frac{\Gamma_{\text{H}}}{\Gamma_{\text{HM12}}} \right]^{1/2} \left[\frac{H(z)}{H_0} \right]^{1/2} h_{70}^{-1} p_{100}^{1/2} T_4^{0.363} (1+z)^{0.2} \times \int_{N_{\text{min}}}^{N_{\text{max}}} \frac{d^2\mathcal{N}}{d \log(N_{\text{HI}}) dz} N_{14}^{1/2} d(\log N_{\text{HI}}). \quad (10)$$

Owing to the n_{H}^2 dependence of neutral fraction in photoionization equilibrium, the factor $\Gamma_{\text{H}}(z)$ enters Equations (8) and (10) as the square root, with a $(1+z)^{2.2}$ dependence that nearly balances the $(1+z)^2$ from the cosmological ratio $[\phi(z)/(1+z)]$ in Equation (7). Two recent *HST* surveys (Tilton et al. 2012; Danforth et al. 2015) probed Ly α absorbers out to $z \approx 0.47$ and found that between 24% and 30% of the baryons reside in the low- z Ly α forest. Equation (10) is consistent with those estimates, particularly with our recommended factor-of-two increase in ionizing background, $\Gamma_{\text{H}}(z) = (4.6 \times 10^{-14} \text{ s}^{-1})(1+z)^{4.4}$ over the range $0 < z < 0.7$.